ARL-TR-10251 ● Dec 2025

Modeling of Actuators for Control Surfaces of a Glide-Body Air Vehicle

by Yan Borden, Daniel Inman, Muthuvel Murugan, and D. Johann Djanal-Mann

NOTICES

Disclaimers

ARL-TR-10251 ● DEC 2025

Modeling of Actuators for Control Surfaces of a Glide-Body Air Vehicle

Yan Borden and Daniel Inman
University of Michigan–Ann Arbor

Muthuvel Murugan and D. Johann Djanal-Mann
DEVCOM Army Research Laboratory

REPORT DOCUMENTATION PAGE

1. REPORT DATE	2. REPORT TYPE	3. DATES COVERED START DATE	3. DATES COVERED END DATE
December 2025	Technical Report	4/16/2024	4/30/2025

4. TITLE AND SUBTITLE
Modeling of Actuators for Control Surfaces of a Glide-Body Air Vehicle

5a. CONTRACT NUMBER	5b. GRANT NUMBER	5c. PROGRAM ELEMENT NUMBER
CA W911NF-22-2-0048		
5d. PROJECT NUMBER	**5e. TASK NUMBER**	**5f. WORK UNIT NUMBER**

6. AUTHOR(S)
Yan Borden, Daniel Inman, Muthuvel Murugan, and D. Johann Djanal-Mann

7. PERFORMING ORGANIZATION NAME(S) AND ADDRESS(ES)	8. PERFORMING ORGANIZATION REPORT NUMBER
DEVCOM Army Research Laboratory ATTN: FCDD-RLA-VA Aberdeen Proving Ground, MD 21005	ARL-TR-10251

9. SPONSORING/MONITORING AGENCY NAME(S) AND ADDRESS(ES)	10. SPONSOR/MONITOR'S ACRONYM(S)	11. SPONSOR/MONITOR'S REPORT NUMBER(S)

12. DISTRIBUTION/AVAILABILITY STATEMENT
DISTRIBUTION STATEMENT A. Approved for public release: distribution unlimited.

13. SUPPLEMENTARY NOTES
ORCIDs: D. Johann Djanal-Mann, 0009-0005-1374-7765; Muthuvel Murugan, 0000-0002-8314-3650; Yan Borden, 0009-0000-1040-9123; Daniel Inman, 0000-0001-6195-1334

14. ABSTRACT
This research examined various smart material actuation systems to provide shape-changing capability for glide-body air vehicles. The morphing surfaces of interest consist of lifting surfaces, forebody, and control surfaces. Metrics included the speed of response of the actuation mechanism as well as the required force and deflection. Several shape memory alloys and piezoceramic materials in various device configurations and combinations were considered with the resulting selection being a piezoelectric stack actuation with a passive hydraulic amplifier. Modeling, numerical simulations, and hardware tests were used to size a piezohydraulic actuator prototype consisting of three piezoelectric stacks and a custom hydraulic stroke amplification stage. This system was manufactured and experimentally characterized. The system dynamics were modeled with a nonsymmetrical Bouc–Wen hysteresis model linked with a fluid model based on momentum conservation. A DC linear actuator was also modeled as a competing solution to compare to the piezohydraulic approach using the same metrics. The DC motor actuator was characterized by estimating the parameters of a simplistic analytical model using experimentally acquired data.

15. SUBJECT TERMS
piezoelectric, control actuation, piezohydraulic actuator, smart actuator, control flap actuator, flight control actuators, Mechanical Sciences

16. SECURITY CLASSIFICATION OF: a. REPORT	b. ABSTRACT	C. THIS PAGE	17. LIMITATION OF ABSTRACT	18. NUMBER OF PAGES
UNCLASSIFIED	UNCLASSIFIED	UNCLASSIFIED	UU	27

19a. NAME OF RESPONSIBLE PERSON	19b. PHONE NUMBER *(Include area code)*
Muthuvel Murugan	(520) 691-5892

STANDARD FORM 298 (REV. 5/2020)
Prescribed by ANSI Std. Z39.18

Contents

List of Figures **iv**

List of Tables **iv**

Acknowledgments **v**

1. Introduction **1**

2. Piezohydraulic Actuator **1**

2.1 Development Background 1

2.2 Actuator Model 2

2.3 Simulations, Prototypes, and Experimental Testing 5

2.3.1 Hysteresis Parameter Estimation 5

2.3.2 Example Full-Scale Actuator Simulation 7

2.3.3 Prototype Actuator Simulation 8

2.3.4 Experimental Prototypes 9

3. DC Motor Actuator **12**

3.1 Physics-Based Model 12

3.2 Parameter Estimation 13

4. Future Work **15**

5. Conclusions **15**

6. References **16**

List of Symbols, Abbreviations, and Acronyms **19**

Distribution List **20**

List of Figures

Figure 1. Simplified schematic of hybrid piezohydraulic actuator. 2
Figure 2. Simplified CAD model of piezohydraulic actuator. 3
Figure 3. Simulink of piezohydraulic actuator analytical model. 5
Figure 4. Test setup for piezo stack hysteresis parameter estimation. 6
Figure 5. Hysteresis loops of Thorlabs PKGA7P1 stack. 6
Figure 6. Simulated and experimental Thorlabs piezoelectric stack displacement. 7
Figure 7. Schematic of control surface.. 8
Figure 8. Simulations of large-scale prototype with dynamic pressure equal to a) 10 kPa and b) 25 kPa. 8
Figure 9. Simulation of small-scale prototype. 9
Figure 10. Components of first piezohydraulic actuator prototype. (Top) from left: narrow piston, casing, and wide piston (bottom). 10
Figure 11. First piezohydraulic prototype assembly. 11
Figure 12. Components of second piezohydraulic actuator prototype. (Top) from left: wide piston, casing, and narrow piston (bottom). 11
Figure 13. Free response of first actuator prototype to ramp actuation. 12
Figure 14. Physics-based model of Ultra Motion actuator in Simulink.............. 13
Figure 15. Experimental data used for estimation of actuator parameters, and simulation using the same reference input signal. 14
Figure 16. Validation of Ultra Motion actuator model with estimated parameters. 14

List of Tables

Table 1. Estimated Bouc–Wen parameters based on experimental data. 6
Table 2. Parameters of full-scale piezohydraulic actuator................................. 7
Table 3. Properties of small-scale piezohydraulic actuator. 9

Acknowledgments

This research supports an Applied Research for the Advancement of Science and Technology Priorities program conducted by ARL in collaboration with the Naval Research Laboratory, Air Force Research Laboratory, and Missile Defense Agency under the sponsorship of the Office of the Under Secretary of Defense for Research and Engineering. We thank Richard McKee, Byron Hall, Lowell Welburn, and Dr. Sun Yi of the North Carolina Agricultural and Technical State University, as well as Dr. Anindya Ghoshal (ARL), for their valuable inputs, support, and collaboration.

1. Introduction

A glide-body air vehicle requires the investigation of various actuation mechanisms, including smart materials-based actuators capable of operating at high temperatures. The initial requirements for the control surface actuation system of one such vehicle were as follows:

- 40 mm maximum deflection of control surface
- 2.5 kN minimum blocked force (based on computational fluid dynamics [CFD]-simulated aerodynamic loading)
- 100 mm/s speed of response
- 100 °C maximum operating temperature

To meet these requirements, two different methods were proposed: a novel piezohydraulic actuator and a commercial brushless DC motor linear actuator.

2. Piezohydraulic Actuator

2.1 Development Background

Development started with exploration of smart materials, such as shape memory alloys and piezoelectric materials as the potential basis for the actuation system. The relatively fast required actuation speed immediately steered the search toward piezoelectric stacks, which can be precisely operated at very high frequencies.[1] Piezoelectric stacks are smart material actuators consisting of layers of singular piezoelectric wafers. When a voltage is applied across a singular wafer, it expands slightly. Combining these elements into a stack effectively sums up the displacement produced by each layer.[1] Typically, piezoelectric stacks can produce displacements on the order of 1–500 µm and blocked forces of up to 80 kN, while the resolution can be as low as 0.5 nm.[2,3] Moreover, piezoelectric stacks can exhibit high bandwidth, which is why they are often used in high-speed or precision applications that do not require large displacements such as microscopy,[4,5] optical mirror positioning,[6,7] and valve control for fluid flow.[8,9] However, the small displacement stroke has mostly confined their use to micro- and nano-applications.

Different mechanisms, such as mechanical and hydraulic, have been used to amplify the stroke of piezoelectric stacks. Mechanical methods include lever, bridge, and Scott–Russell mechanisms.[10–12] Hydraulic amplification motors use piezoelectric stacks as high-frequency pumps.[10,13] Stepped piezoelectric motors, such as inchworm and walking motors, activate the piezo stacks in a high-frequency pattern, which results in a cumulative linear movement of an output shaft.[14,15]

While most of these systems successfully amplify the piezoelectric stack displacement to the millimeter range, they often sacrifice a significant amount of blocked force that the piezoelectric stacks have to offer. Therefore, these devices cannot be used in applications where a kN-range force is needed. Direct hydraulic amplification of piezoelectric stacks had been experimented with before, but previous works failed to reach a high output force.[16,17] Furthermore, no complete analytical model of similar actuators has been presented.

2.2 Actuator Model

The piezohydraulic actuator has two main components: piezoelectric stacks and a hydraulic amplification stage. To amplify the displacement of the piezoelectric stacks to the millimeter range, it is proposed to use a hydraulic stage that would magnify the small stroke of the stacks by exploiting mass conservation of fluid flow through a channel. A simple schematic of the actuator is shown in Figure 1. The piezoelectric stacks push the fluid through a narrowing channel in the flow, which creates a large displacement at the output cylinder of the actuator. Assuming the pressure in the fluid to be equal everywhere due to Pascal's principle, the force output of the actuator is reduced by the same factor that the displacement is amplified. To mitigate this effect, more than one stack is used at the base of the actuator to increase the force output of the actuator. The precision of the actuator is decreased, with the resolution being magnified by the same factor as the displacement, but, theoretically, the entire actuator should still be accurate to tens of micrometers due to the inherently high precision of the piezo stacks. In this way, the design preserves the quick and precise response of the piezoelectric stacks, while amplifying the displacement to the millimeter range. A section view of a simplified 3D CAD model of the device is shown in Figure 2.

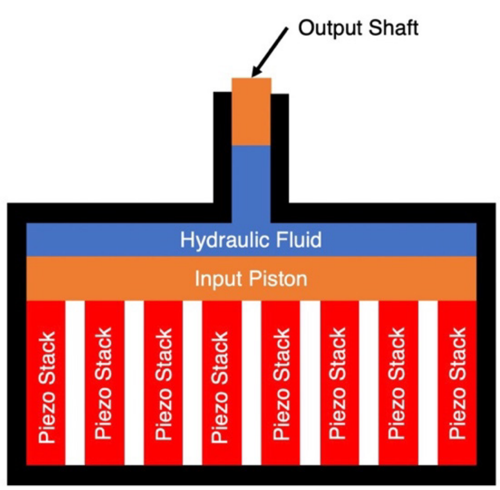

Figure 1. Simplified schematic of hybrid piezohydraulic actuator.

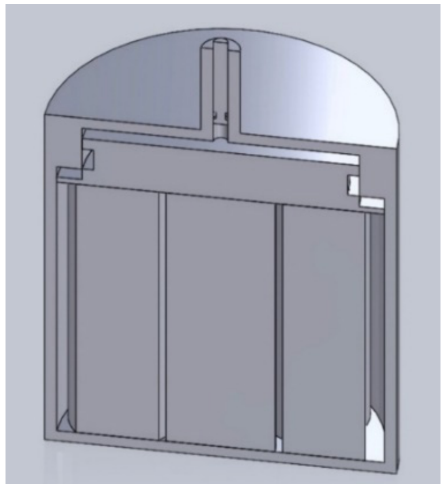

Figure 2. Simplified CAD model of piezohydraulic actuator.

The first part of the analytical model of the actuator is the set of equations for the piezoelectric stacks, which are known to experience hysteresis. A nonsymmetrical Bouc–Wen model[18] used to account for nonlinear behavior is,

$$x_{free}(t) = d_{33}v(t) + h(t) \tag{1}$$

$$\dot{h}(t) = \{\alpha - [\beta\, sgn(\dot{v}(t)h(t)) + \gamma]\, |h(t)|^{n}\}\dot{v}(t) + \delta v(t)\, sgn(\dot{v}(t)) \tag{2}$$

In Equations 1 and 2, x_{free}, d_{33}, and $v(t)$ are the free displacement of the piezo stacks, the piezoelectric coefficient, and the applied voltage, respectively, while $\alpha, \beta, \delta, \gamma, n$ are parameters of the hysteresis model, and $h(t)$ is the nonlinear component of the free displacement. The displacement of a single piezo stack ($x(t)$) with an applied load ($F_{applied,piezo}$) can then be calculated using the stiffness of the piezoelectric stacks, k_s by

$$x(t) = x_{free} - \frac{F_{applied,piezo}}{k_s} \tag{3}$$

This displacement of the piezo stacks is then amplified due to mass conservation through the narrowing given below, where $R = \frac{A_{wide}}{A_{narrow}}$ is the amplification ratio based on the cross-sectional areas of the wide and narrow channels:

$$x(t)A_{wide} = y(t)A_{narrow} \tag{4}$$

$$y(t) = \frac{A_{wide}}{A_{narrow}}x(t) = Rx(t) \tag{5}$$

The next component of the model is the calculation of the force applied to each piezo stack ($F_{applied,piezo}$). Assuming that the force is distributed equally across all stacks, and using Newton's third law for the wide cylinder (m_{wide}), $F_{applied,piezo}$

can be related to the pressure force applied to the wide cylinder (F_{wide}) using the number of stacks (n_{stacks}) with Equation 6:

$$m_{wide}\ddot{x}(t) = n_{stacks}F_{applied,piezo} - F_{wide} \tag{6}$$

$$F_{applied,piezo} = \frac{m_{wide}\ddot{x}(t) + F_{wide}}{n_{stacks}} \tag{7}$$

Next, the momentum equation for a narrowing in the fluid[19] can be manipulated to relate the force applied to the narrow piston (F_{narrow}) to F_{wide}:

$$p_{wide} - p_{narrow} = \frac{\dot{m}^2}{2\rho}\left(\frac{1}{A_{narrow}^2} - \frac{1}{A_{wide}^2}\right) + K_{loss}\frac{\dot{m}^2}{2\rho A_{narrow}^2} \tag{8}$$

$$p_{narrow} = p_{wide} + \rho\frac{\dot{x}^2}{2}(1 - R^2 - K_{loss}R^2) \tag{9}$$

$$F_{wide} = RF_{narrow} + A_{wide}\rho\frac{\dot{x}^2}{2}(R^2 + K_{loss}R^2 - 1) \tag{10}$$

In Equations 8–10, p_{wide} and p_{narrow} represent the pressures in the wide and narrow channels, respectively, while K_{loss} is a nondimensional loss factor due to the constriction in the flow, and ρ is the density of the fluid. Notably, Equation 10 reduces to Pascal's principle (pressure transmitted equally in fluid) when there is no fluid movement. Conceptually, the loss of pressure due to fluid flow decreases the capability of the actuator to counteract load at the output. Combining Equations 1–5, 7, and 10 results in the Simulink model shown in Figure 3, where the seal forces are also incorporated into F_{wide} and F_{narrow}.

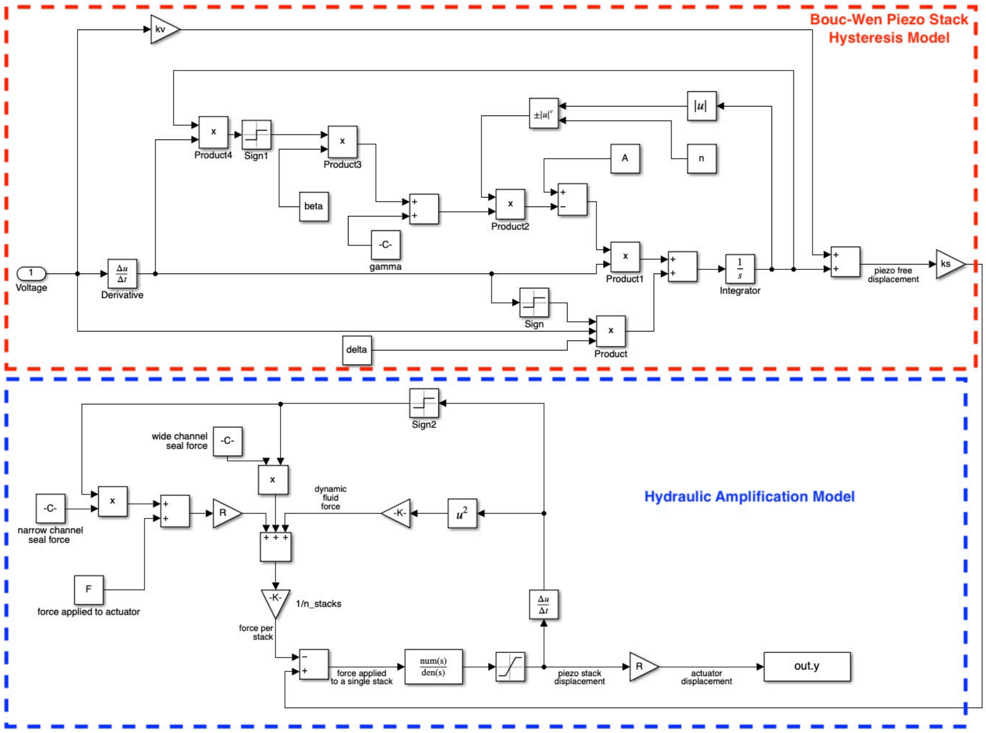

Figure 3. Simulink of piezohydraulic actuator analytical model.

2.3 Simulations, Prototypes, and Experimental Testing

2.3.1 Hysteresis Parameter Estimation

Experimental voltage-displacement data was obtained by actuating a Thorlabs PKGA7P1 stack[3] with voltage sine waves of increasing frequency, which were provided by a Thorlabs MDT693B open-loop piezo controller. The corresponding displacement of the stack was measured by a Keyence LJ-V7300 laser sensor, while the voltage was measured using a voltage divider circuit. The voltage and displacement data were then acquired using an NI USB-6009 data acquisition device. The experimental setup is shown in Figure 4. The corresponding hysteresis loops are shown in Figure 5. The Bouc–Wen parameters for the PK4GA7P1 stack were then determined using the Simulink Parameter Estimation app and are shown in Table 1. A plot of the simulated versus experimental data is shown in Figure 6.

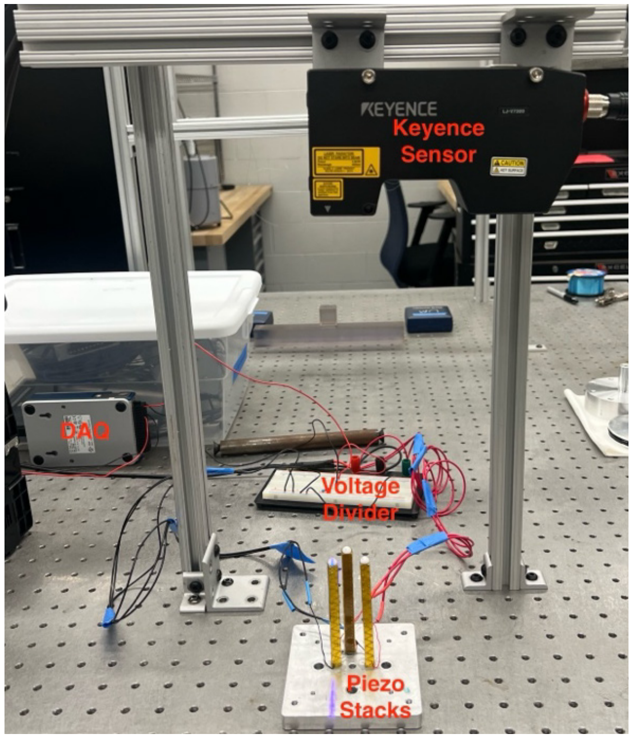

Figure 4. Test setup for piezo stack hysteresis parameter estimation.

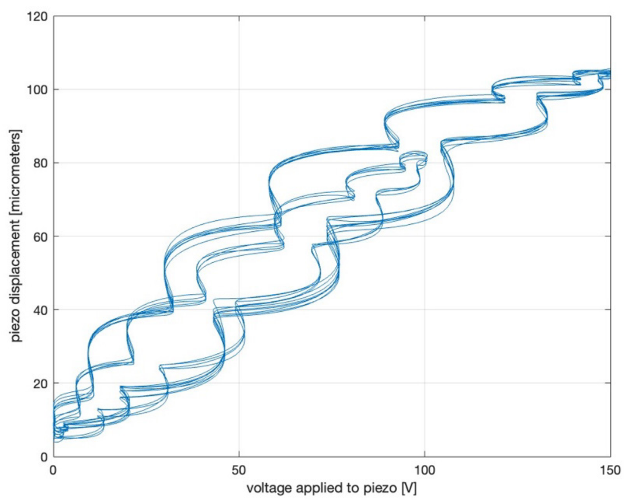

Figure 5. Hysteresis loops of Thorlabs PKGA7P1 stack.

Table 1. Estimated Bouc–Wen parameters based on experimental data.

Bouc–Wen parameters	Estimated values
α	–2.23e–7
β	0.134
δ	–5.46e–8
γ	0.0755
n	1.14
d_{33}	8.15e–7

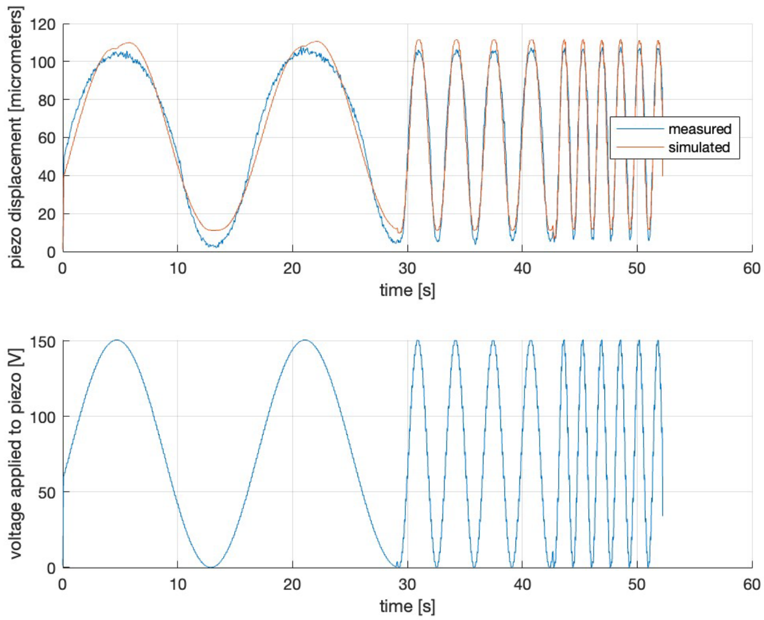

Figure 6. Simulated and experimental Thorlabs piezoelectric stack displacement.

2.3.2 Example Full-Scale Actuator Simulation

The various parameters of a piezohydraulic actuator sized for a maximum free deflection of 50 mm, with 10 high-power piezoelectric stacks (Physik Instrumente [PI] 056.90), and a minimum 2.5 kN blocked force are shown in Table 2. An experimental version of this configuration proved unrealistic to build due to the high cost of the PI 056.90 stack of around $20,000.[2] Therefore, performance of this actuator was estimated using numerical simulations (Simulink of Figure 3). It was also assumed that the hysteresis parameters between the PI 056.90 and Thorlabs PKGA7P1 were approximately equal for the simulations. The hinged control surface attached at the tip to the actuator was assumed to have dimensions equal to 15 × 10 × 0.0625 inches with negligible rotational inertia and constant pressure equal to 10 and 25 kPa, as consistent with the dynamic pressures for a glide-body air vehicle cruising at Mach 10 at altitudes of 40 and 35 km, respectively (schematic shown in Figure 7). The wide and narrow seals were assumed to generate 10 and 0.2 N friction forces, respectively. Example resulting open-loop simulations are shown in Figure 8.

Table 2. Parameters of full-scale piezohydraulic actuator.

Parameters	Values
Piezoelectric stack stiffness (k_s)	4.33e8 N/m
Amplification ratio (R)	277
Piezoelectric coefficient (d_{33})	1.8e–7 m/V
Maximum free displacement	50 mm
Blocked force	2.82 kN
Number of piezo stacks	10

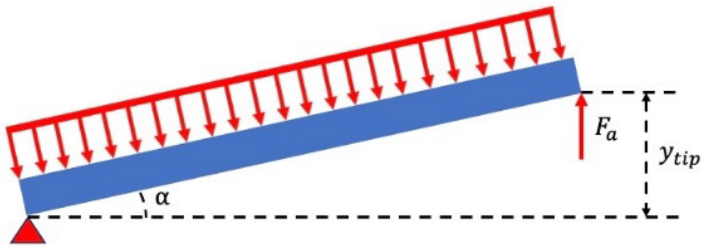

Figure 7. Schematic of control surface.

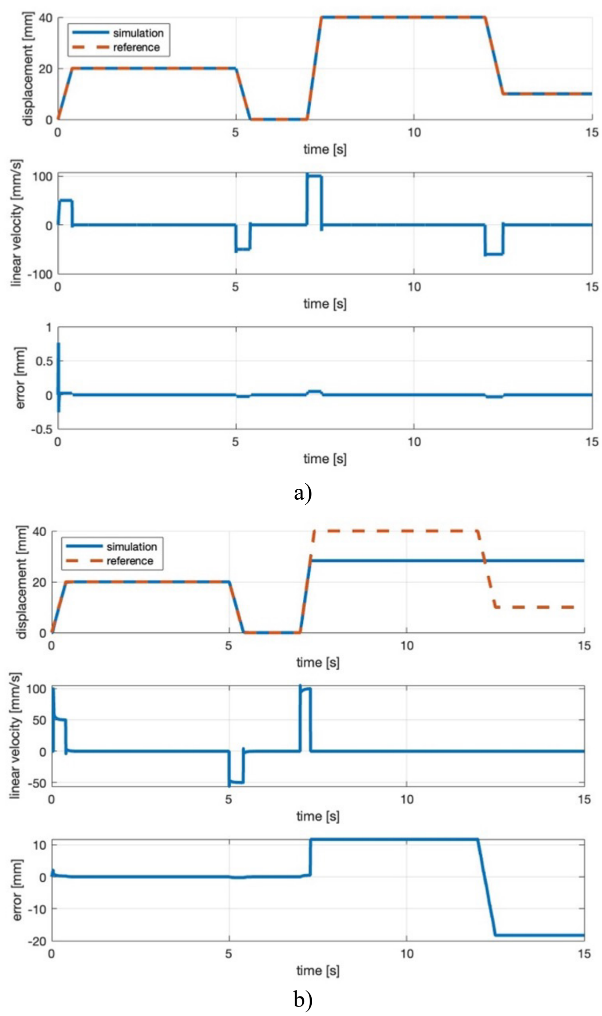

Figure 8. Simulations of large-scale prototype with dynamic pressure equal to a) 10 kPa and b) 25 kPa.

2.3.3 Prototype Actuator Simulation

A small-scale prototype of the actuator was proposed with three of the Thorlabs PK4GA7P2 stacks, which were used for the hysteresis model estimation. Properties of this actuator are shown in Table 3. The wide and narrow seals were assumed to generate 10 and 0.2 N friction forces, respectively. An open-loop simulation of the actuator driven by sine waves of increasing frequency is shown in Figure 9. Notably, the actuator cannot achieve its maximum theoretical displacement due to losses associated with the fluid and seal friction.

Table 3. Properties of small-scale piezohydraulic actuator.

Parameters	Values
Piezoelectric stack stiffness (k_s)	1.96e7 N/m
Wide channel diameter	0.375 inches
Narrow channel diameter	3.750 inches
Amplification ratio (R)	106
Piezoelectric coefficient (d_{33})	6.7e–7 m/V
Maximum theoretical free displacement	10 mm
Blocked force	58.8 N
Number of piezo stacks	3

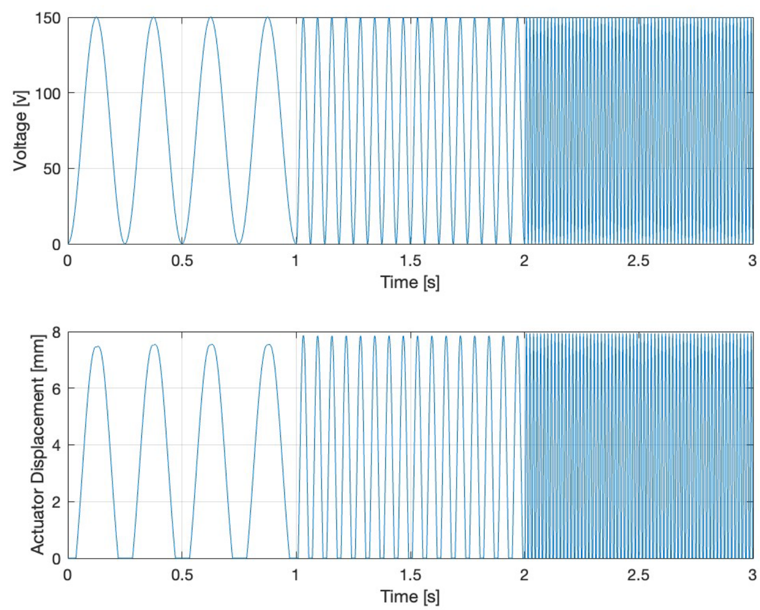

Figure 9. Simulation of small-scale prototype.

2.3.4 Experimental Prototypes

Two iterations of experimental small-scale prototypes of the piezohydraulic actuator were constructed. Both prototypes have the properties of Table 3 and consist of three Thorlabs PK4GA7P1 piezoelectric stacks and custom 6061-T6 aluminum hydraulic stages, which comprise the wide and narrow channel pistons, as well as the casing. ISO 15 hydraulic fluid was used in the experimental setup due to the low viscosity of this oil at room temperature. The difference between the prototypes was in the type of seals: spring-energized PTFE seals were used in the first prototype, while standard SAE AS568 PTFE O-rings[20] were implemented in the second iteration for the purpose of replacing the seals quicker if the need arose. Furthermore, a load attachment hole in the narrow piston and an air relief valve in the input piston were added in the second prototype. The piezoelectric stacks were attached to the wide cylinder using specially made bearings from Thorlabs. This ensures that the force from the stacks is transmitted in the axial direction. Components of both prototypes are shown in Figures 10–12.

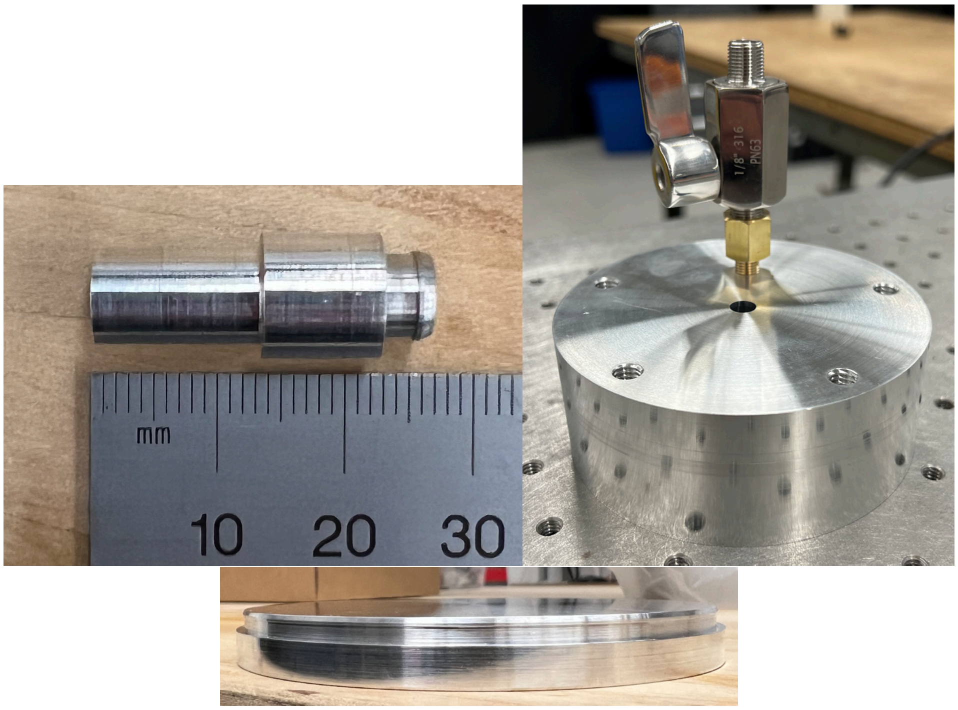

Figure 10. Components of first piezohydraulic actuator prototype. (Top) from left: narrow piston, casing, and wide piston (bottom).

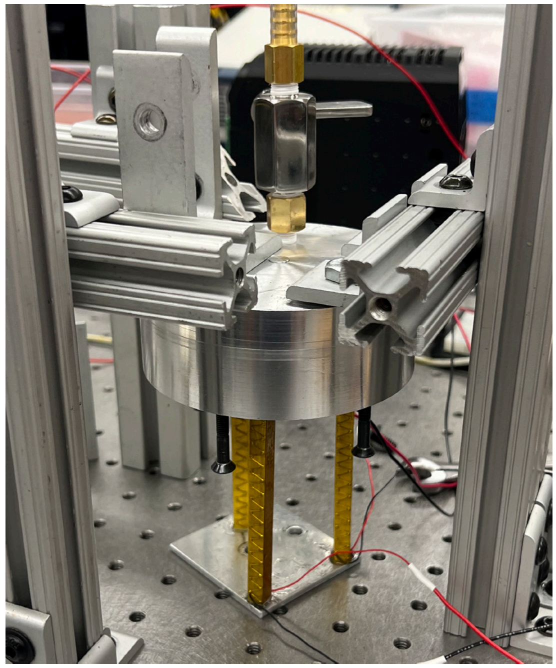

Figure 11. First piezohydraulic prototype assembly.

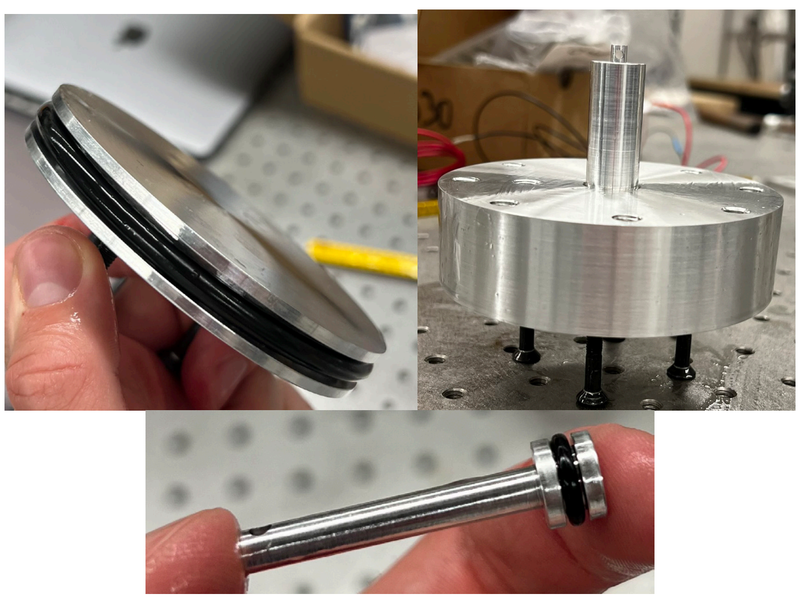

Figure 12. Components of second piezohydraulic actuator prototype. (Top) from left: wide piston, casing, and narrow piston (bottom).

The free response of the first small-scale prototype, which was measured using the same Keyence laser displacement sensor, is shown in Figure 13. As predicted in the simulation, the prototype could not reach the maximum theoretical displacement of 10 mm; the simulation predicted around 7.5 mm, while the maximum experimental value was approximately 7 mm. Additionally, the spring-energized seals seemed to provide a significant amount of resistance, which meant that the response was "stepped." This was part of the motivation for replacing the seal type in the second prototype. The first prototype also lacked a return mechanism, which is why it had to be manually reset to its starting position. Experimental testing of the second prototype is planned to be conducted soon.

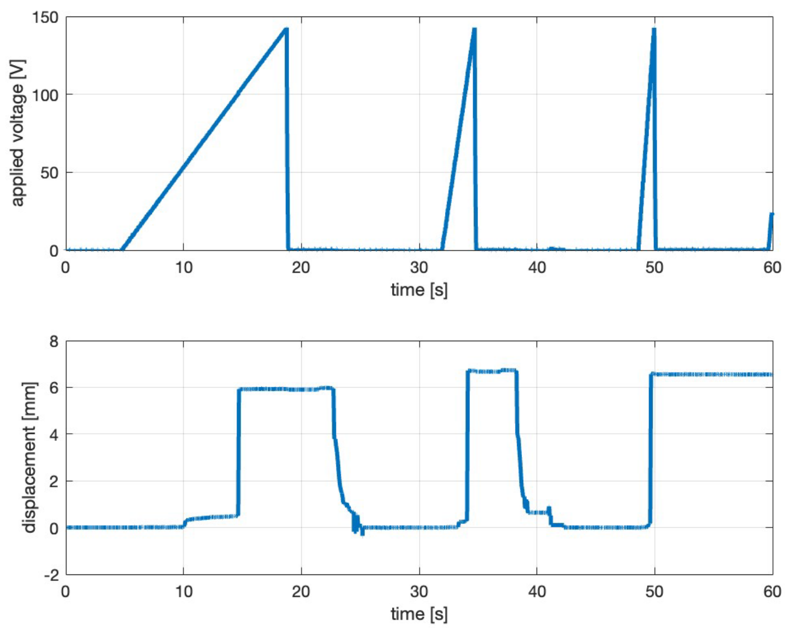

Figure 13. Free response of first actuator prototype to ramp actuation.

3. DC Motor Actuator

The main alternative to the piezohydraulic actuator is a linear brushless DC stepper motor actuator manufactured by Ultra Motion (model AMCX8B-B0M1).[21] Essentially, this actuator works by converting the rotational motion of a DC electric motor into linear motion using a lead screw. To facilitate high-quality simulations, accurate modeling of the Ultra Motion actuator was required.

3.1 Physics-Based Model

Based on the description of the analytical model from the manufacturer, the actuator plant could be split up into two components—a built-in 1.25-kHz proportional–integral–derivative (PID) controller that takes in a reference position command and regulates the current on the windings of the motor, and the actuator physics. The actuator physics were assumed to be in the following form,[22] where J is the rotor inertia, k_t is torque constant, λ is the motor damping, $\omega(t)$ is the angular velocity of the rotor, $l_{bs} = 2$ mm is the known screw lead, $i(t)$ is the current on the motor (control variable), and $v(t)$ is the linear velocity of the actuator:

$$J\dot{\omega}(t) + \lambda\omega(t) = k_t i(t) \tag{11}$$

$$\dot{v}(t) = -\frac{\lambda}{J} v(t) + \frac{l_{bs} k_t}{2\pi J} i(t) \tag{12}$$

The coefficients in front of the state and control variables are ratios between unknown parameters; therefore, Equation 12 can be rewritten using two new identifiable parameters (c_1 and c_2):

$$\dot{v}(t) = c_1 v(t) + \frac{l_{bs}}{2\pi} c_2 i(t) \tag{13}$$

Converting Equation 13 to discrete form,

$$v[k+1] = e^{c_1 \Delta t}\, v[k] + \frac{e^{c_1 \Delta t} - 1}{c_1} \frac{l_{bs}}{2\pi} c_2 i[k] \tag{14}$$

The combined actuator plant model was then built-in in Simulink, as shown in Figure 14, where the state-space block represents Equation 14. The default PID gains were known from the actuator data sheet.

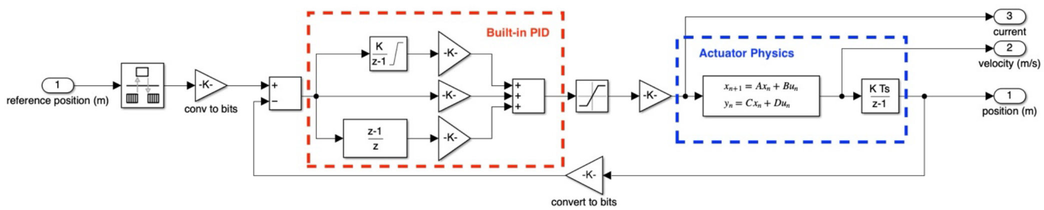

Figure 14. Physics-based model of Ultra Motion actuator in Simulink.

3.2 Parameter Estimation

Actuator response data was obtained by teams at North Carolina Agricultural and Technical State University and the U.S. Army Combat Capabilities Development Command (DEVCOM) Army Research Laboratory (ARL), and the parameter estimation toolbox was used for identification of parameters c_1 and c_2. The input for the estimation was the reference position signal, while the output was the externally measured position. The estimation was carried out based on the step response shown in Figure 15 with further validation conducted using periodic reference data as shown in Figure 16. The steady-state oscillations in Figure 15 were the result of sensor vibration, not due to the actuator physics. The values for the c_1 and c_2 parameters were estimated to equal –25.5552 and 2987.02, respectively. The simulation comes sufficiently close to the experimental data, fulfilling the criteria for an accurate actuator model.

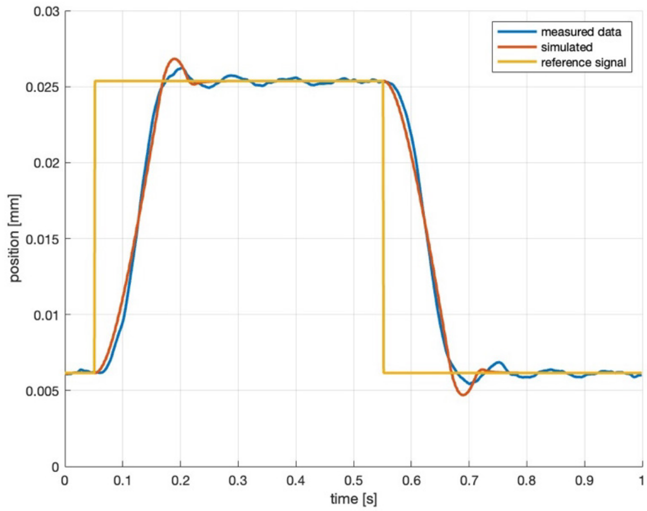

Figure 15. Experimental data used for estimation of actuator parameters, and simulation using the same reference input signal.

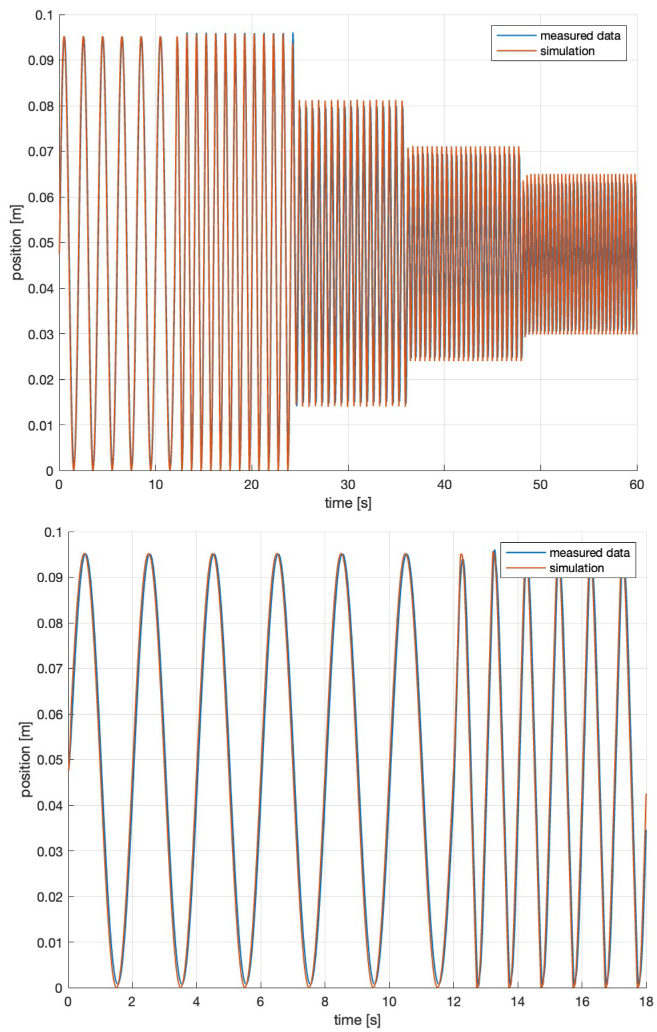

Figure 16. Validation of Ultra Motion actuator model with estimated parameters.

4. Future Work

The work on the second small-scale prototype of the piezohydraulic actuator will soon be completed. This will, hopefully, allow more rigorous experimental testing. If sufficient resources are available, a full-scale (with high-power piezo stacks) piezohydraulic actuator prototype should be constructed. In this way, an experimental comparison to the Ultra Motion actuator could be completed. Furthermore, testing of the Ultra Motion actuator with a representative control surface and aerodynamic loading would validate use of the actuator in the given application.

5. Conclusions

The presented work outlines two models of actuators that could potentially be used for control surface actuation in a glide-body air vehicle. The developed piezohydraulic actuator shows promise for this application, but further testing is needed to validate its use. The construction of piezohydraulic prototypes has also been nontrivial, which has slowed down its development. The DC motor linear actuator, however, is readily available for use and the model presented can be used for simulations or for tuning of the actuator built-in PID parameters to improve its performance.

6. References

1. Leo DJ. Common operating modes of a piezoelectric transducer. Engineering analysis of smart material systems. John Wiley & Sons; 2007. Ch. 4. p. 150–157.

2. Piezoelectric transducers & actuators. Physik Instrumente (PI) SE & Co. KG.; c2025. https://www.physikinstrumente.com/en/products/piezoelectric-transducers-actuators

3. Discrete piezoelectric stacks, 5.2 µm to 100.0 µm travel. Thorlabs, Inc; c2025. https://www.thorlabs.com/thorproduct.cfm?partnumber=PK4GA7P1

4. Guliyev E et al. Quasi-monolithic integration of silicon-MEMS with piezoelectric actuators for high-speed non-contact atomic force microscopy. Meas Sci Technol. 2011;23(7):1–8. https://doi.org/10.1088/0957-0233/23/7/074012

5. Shimizu M et al. An ultrafast piezoelectric Z-scanner with a resonance frequency above 1.1 MHz for high-speed atomic force microscopy. Rev Sci Instrum. 2022;91(1):1–10. https://doi.org/10.1063/5.0072722

6. Ran B et al. Design and analysis of a reactionless large-aperture fast steering mirror with piezoelectric actuators. Appl Opt. 2020;59(4):1169–1179. https://doi.org/10.1364/AO.379344

7. Sherrit S et al. Characterization of multilayer piezoelectric stacks down to 100K. IEEE Open J Ultrason Ferroelectr Freq Control. 2022;2:65–82. https://doi.org/10.1109/OJUFFC.2022.3173919

8. Pluta J, Sibielak M. The application of a piezoelectric stack for control of small flow intensity hydraulic fluid. Proceedings of the 13th International Carpathian Control Conference (ICCC); 2012. p. 573–577. https://doi.org/10.1109/CarpathianCC.2012.6228710

9. Han C, Choi S, Han Y. A piezoelectric actuator-based direct-drive valve for fast motion control at high operating temperatures. Appl Sci. 2018;8(10):1–14. https://doi.org/10.3390/app8101806

10. Vo TV, Lubecki TM, Chow WT, Gupta A, Li KH. Large-scale piezoelectric-based systems for more electric aircraft applications. Micromachines. 2021;12(2):140. https://doi.org/10.3390/mi12020140

11. Wei H et al. Development of piezo-driven compliant bridge mechanisms: general analytical equations and optimization of displacement amplification. Micromachines. 2017;8(8):238. https://doi.org/10.3390/mi8080238

12. Chen CM, Hsu YC, Fung RF. System identification of a Scott–Russell amplifying mechanism with offset driven by a piezoelectric actuator. Appl Math Model. 2011;36(6):2788–2802. https://doi.org/10.1016/j.apm.2011.09.064

13. Mauck L, Oates W, Lynch C. Piezoelectric hydraulic pump development. 41st Structures, Structural Dynamics, and Materials Conference and Exhibit; 2000 Oct. Vol. 11, no. 10. https://doi.org/10.2514/6.2000-1789

14. Miesner JE, Teter JP. Piezoelectric/magnetostrictive resonant inchworm motor. SPIE Proceedings. 1994;2190(1):520–527. https://doi.org/10.1117/12.175212

15. PiezoWalk piezo motors. Physik Instrumente (PI) SE & Co. KG.; c2025. https://www.pi-usa.us/en/expertise/technology/piezoelectric-drives/piezowalk-piezo-motors

16. Tang H, Li Y, Xiao X. Development and assessment of a novel hydraulic displacement amplifier for piezo-actuated large stroke precision positioning. 2013 IEEE International Conference on Robotics and Automation; 2013; Karlsruhe, Germany. p. 1409–1414. https://doi.org/10.1109/ICRA.2013.6630755

17. Yoon H et al. A millimeter-stroke piezoelectric hybrid actuator using hydraulic displacement amplification mechanism. 2006 IEEE International Symposium on Industrial Electronics; 2006; Montreal, QC, Canada. p. 2809–2813. https://doi.org/10.1109/ISIE.2006.296060

18. Zhu W, Wang DH. Non-symmetrical Bouc–Wen model for piezoelectric ceramic actuators. Sens Actuators A. 2012;181:51–60. https://doi.org/10.1016/j.sna.2012.03.048

19. Sudden area change (TL). The MathWorks, Inc; c2025. https://www.mathworks.com/help/hydro/ref/suddenareachangetl.html

20. SAE AS568F. Aerospace size standard for O-rings. SAE International; 2020 Sep 29.

21. A-series: electromechanical linear actuator with fully integrated phase index control system. Ultra Motion; c2025. https://ultramotion.com/servo_cylinder/ultra-motion-servo-cylinder-manual.pdf

22. DC motor. The MathWorks, Inc; c2025. https://www.mathworks.com/help/sps/ref/dcmotor.html

List of Symbols, Abbreviations, and Acronyms

3D	Three-Dimensional
ARL	Army Research Laboratory
CAD	Computer-Aided Design
CFD	Computational Fluid Dynamics
DC	Direct Current
DEVCOM	U.S. Army Combat Capabilities Development Command
DoD	Department of Defense
ISO	International Organization for Standardization
PI	Physik Instrumente
PID	Proportional–Integral–Derivative
PTFE	Polytetrafluoroethylene
SAE	Society of Automotive Engineers

1 (PDF)	DEFENSE TECHNICAL INFORMATION CTR DTIC OCA
1 (PDF)	DEVCOM ARL FCDD RLB CI TECH LIB